Arch. Metall. Mater. **69** (2024), 3, 881-890

DOI: https://doi.org/10.24425/amm.2024.150908

A.A. KHAN[1], M.S. KAISER[2*]

WEAR PROPERTIES ANALYSIS ON Al-BASED AUTOMOTIVE ALLOY WITH VARIED LEVELS OF Si IN DRY, 3.5% NaCl AND SEAWATER CORROSIVE ENVIRONMENTS

The wear tests of aluminum based automotive alloys with different Si content in 3.5% NaCl, seawater and dry sliding environment are carried out. A conventional pin-on-disc wear apparatus is used at 2.55 MPa pressure and 0.51 m/s speed for a sliding distance of 923.2 m. The results show that the wear rate and friction coefficient of the alloy decreases with the increase of silicon content up to the eutectic point in all sliding environments. Among the different Si-rich intermetallics formed, especially Mg_2Si strengthens the alloys. It is more prominent in the case of a corrosive environment through creating MgO plus SiO_2 layers, which protect the corrosive wear and reduce the friction coefficient. Wear test surfaces have shown that Si addition makes the alloys wear-resistant with smooth abrasive grooves covered with oxides.

Keywords: Al-Si alloy; corrosive wear; friction coefficient; worn surfaces; oxide formation

1. Introduction

According to the aluminum alloy designation system it is called 4xxx series alloy when silicon is considered as the principal alloying element [1,2]. Replacing cast iron with Si-doped Al-alloy as engine material has reduced fuel consumption as the weights of engine components are reduced [3]. The 4xxx series alloys are extensively used in the automobile sector for making parts like engine heads, pistons blocks, connecting rods, pistons, and liners, *etc*., since their improved properties. Considering their improved properties, these alloys are also considered for machine manufacturing, aviation, transportation, construction, and other vital sectors. They are also used in complex shapes castings such as cover plates, motor shells, brackets, etc. The alloy with 12.6 wt.% Si is referred to as eutectic Al-Si alloy. The higher and lower levels of the Si content in the alloys are termed hyper and hypo-eutectic Al-Si alloys respectively [4,5]. According to existing research, alloying elements like Cu, Mg, Fe, Ni, Zn, *etc.*, are used in this type of Al-based automotive alloy to enhance certain properties. Al-Si alloys containing Cu and Mg respond to age hardening [6-9]. In most of the automotive materials, 0.8-1.5% Cu, 0.8-1.3% Mg, 0.8-1.3% Ni, <0.7% Fe, <0.3% Mn are present, whereas the wt.% of Si varies in a wide range (11-26%) [4]. Adding an element to improve one property of the alloy can have unintended effects on other properties. Not only are the elements important, but their amount is another factor that controls the properties of the alloys. One of the concerning properties of this type of alloy is wear behavior. Wear means the elimination of material from the sliding surfaces causing continuous material loss. High wear-resistant material provides a better engine life. Al-Si has high-quality wear resistance due to the formation of several intermetallics such as Al_2Cu, Mg_2Si, β-Al_5FeSi, *etc.*, fine intermetallics [10,11]. When the amount of Si is increased, keeping other alloying elements constant, the amount of Si-rich intermetallics also increases, which strengthens the material and increases both wear and corrosion resistance [12,13]. However, wear with corrosion induces failure during service. Since corrosion is greatly affected by the surroundings and frequently occurs with wear, material loss is considerably increased. Therefore, the root cause of the failure leads to improvements in the design of components [14,15]. The engine material can be exposed to NaCl and seawater frequently. There are small amounts of NaCl dissolved in cooling water. Again, the engine's radiator is often filled with local tap water, where NaCl is present. On the other hand, the engines in marine applications get into contact with seawater frequently.

Many studies have been made to understand the surface behavior in sliding contact and the mechanism under various

[1] BANGLADESH UNIVERSITY OF ENGINEERING AND TECHNOLOGY, DEPARTMENT OF MECHANICAL ENGINEERING, DHAKA-1000, BANGLADESH
[2] INTERNATIONAL UNIVERSITY OF BUSINESS AGRICULTURE AND TECHNOLOGY, INNOVATION CENTRE, DHAKA-1230, BANGLADESH

* Corresponding author: dkaiser.res@iubat.edu

parameters like alloy composition, applied pressure, sliding speed, counter surface, sliding environment, *etc*. Si-added Al-based alloys are extensively used in different automobiles, shipbuilding, and aerospace engine structural applications. Tribological properties are important for materials under a relative motion, but these properties depend strongly on working conditions. Besides operating parameters, operating media, such as dry, wet, lubricant, corrosive solution, *etc.* are also important working conditions [16-18]. Thus, it becomes necessary to study the tribological characteristics of these alloys under different environments. In this exploration, the wear of Al-based automotive alloys with different levels of Si is assessed, keeping other alloying elements constant, intending to determine the role of Si when exposed to a 3.5% NaCl solution and seawater sliding environment. Dry sliding wear condition is also considered for comparing the wear behavior with the other two conditions.

2. Experimental

To study the role of Si on the wear behavior of aluminium based automotive alloys, the following five alloys were cast with Si varied at 0.2, 3.5, 6.1, 12.7, and 17.9 wt.% while keeping 2.2Cu, 0.8Mg and 0.3Fe nearly constant. The chemical compositions of the developed alloys were evaluated by the spectrochemical method as

Alloy 1: Al-0.2Si-2.2Cu-0.8Mg-0.2Fe
Alloy 2: Al-3.5Si-2.3Cu-0.8Mg-0.3Fe
Alloy 3: Al-6.1Si-2.1Cu-0.8Mg-0.3Fe
Alloy 4: Al-12.7Si-2.1Cu-0.8Mg-0.3Fe
Alloy 5: Al-17.9Si-2.2Cu-0.8Mg-0.3Fe

and some Ni, Pb, Mn, Zn, and Ti as trace elements naturally added from the environment.

For developing these alloys, aluminium, copper, magnesium, and the master alloy of Al-50%Si were melted in a graphite crucible using a natural gas-fired pit furnace. An appropriate flux cover was used to avoid oxidation during melting. Casting was done at 700°C in a mild steel mold of 20 mm×200 mm×300 mm, preheated at 250°C. The homogenization of the cast alloys occurred in a muffle furnace at 450°C for 12 hours, and they were air-cooled subsequently to alleviate internal stresses. The alloys were then solutionized at 535°C for two hours and quenched in salt ice water to get a super-saturated region of a single phase. A Vickers hardness testing machine with a load of 1 kg was applied on the surface of a sample for 10 seconds for ten successive readings, and the average value was considered as the hardness of that sample. The density of each alloy was calculated from the chemical composition. The solution-treated cast alloys were machined to 14 mm length and 5 mm diameter as samples for wear study. The samples were kept at 200°C for 240 minutes for age hardening to achieve the peak-aged condition [19-21]. A pin-on-disc wear testing apparatus was used to estimate the wear and frictional behavior of the alloys maintaining the ASTM G99-05 standard under the stated environments [22]. The pin-sized sample was pressed against a stainless-steel disc with a 50 N load, and a 200 rpm horizontal rotation on a track of 49 mm diameter was provided to the disc for the corresponding wear test. Each test was performed for a fixed period of 30 minutes. As a result, the calculated sliding distance was 923.2 m, along with the pressure and speed of 2.55 MPa and 0.51 m/s, respectively. The hardness and roughness of the stainless-steel disc were around RC 95 and 0.40 μm, respectively. A minimum of nine experiments were conducted for each identical state under ambient conditions at 22°C and 70% humidity. Average values were considered for making graphs.

The tests were done under dry sliding conditions, and 3.5% NaCl solution and a seawater environment. The 3.5% NaCl solution was prepared by dissolving analytical reagent grade sodium chloride powder with deionized water, which can be considered as simulated seawater, as NaCl is around 3.5% in seawater [23]. The seawater is collected from the Bay of Bengal, in the vicinity of Saint Martin's Island in Bangladesh. The properties of the seawater were determined in our laboratory. The pH of the seawater was 7.14, the total dissolved solids (TDS) was around 28000 mg/L, the dissolved oxygen was 7.29 mg/L, the sulfate ion present was 1320 mg/L, the TSS, turbidity, and electric conductivity were 48 mg/L, 76.9 NTU, and 45000 μS/cm respectively. Throughout the experiment, in NaCl and seawater environments, drip-type single-point lubrication was maintained at the contact interface between the sample and the stainless-steel counter plate.

The following equations determined the wear rates and friction coefficients:

$$\Delta w = w_{initial} - w_{final} \tag{i}$$

$$s.w.r. = \frac{\Delta w}{S.D. \times L} \tag{ii}$$

$$\mu = \frac{F}{L} \tag{iii}$$

where,

$w_{initial}$ – the weight of the sample before wear, g;
w_{final} – the weight of the sample after wear, g;
Δw – the weight loss of the sample during the wear, g;
$S.D.$ – the sliding distance run during wear test, m;
L – the normal load applied on the surface, N;
$s.w.r.$ – specific wear rate, g/Nm;
μ – coefficient of friction;
F – frictional force acting on the surface, N.

The sliding distance was determined from the track diameter and the speed of rotation of the stainless-steel disc.

A USB digital microscope was utilized for the microstructural observation of the surfaces before wear, after wear and the abrasive wear particles of the samples. The SEM and EDX analyses were done using a JEOL scanning electron microscope. The wear testing apparatus, the prepared sample, and counter disc are shown in Fig. 1.

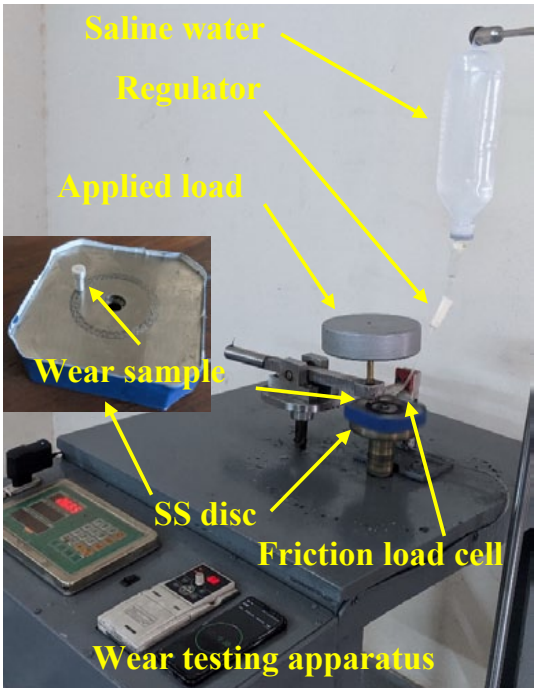

Fig. 1. Photographs of wear testing machine set up with wear sample and friction disc

3. Results and discussion

3.1. Physical and mechanical properties

Fig. 2 shows the variation of density and microhardness of the Al-based automotive alloys with the concentration of Si at the peak aged condition. The alloy with lower silicon content shows the highest density, and it is decreased with the addition of Si. The Al-based experimental alloys contain the elements Cu, Mg, Fe, *etc.*, similar in amount but the Si level varies for different alloys. The variation of density is attributed to the fact that the molecular weight, thus the density of Si, is lower than Al.

Similarly, with increasing the Si content, the hardness increases, as Fig. 2 depicts. This trend is attributed to the strong

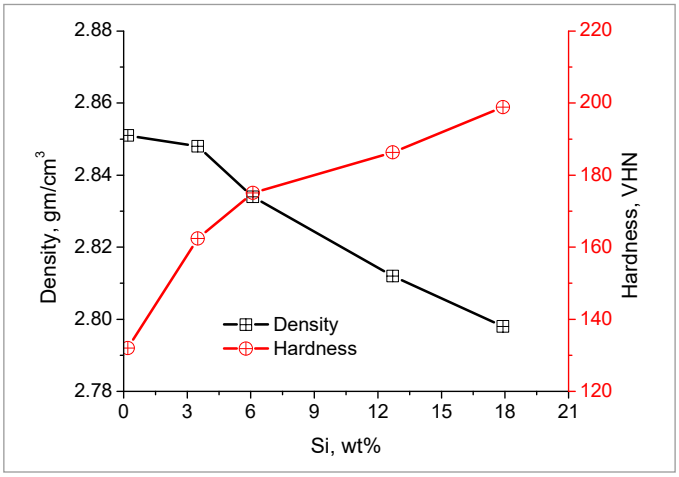

Fig. 2. Variation of density and hardness with Si content of the experimental Al-based automotive alloys

strengthening ability of metastable Si-rich precipitates. Different intermetallics are formed in the Al-Si alloys as they contain different alloying elements. However, the principal strengthening precipitate is Al_2Cu occurring in the form of plates, Mg_2Si, and a small number of hard phases, Al_5FeSi. A higher level of Si produces a higher amount of Si-rich intermetallics resulting in higher hardness [24,25].

3.2. Wear behaviour

The influences of Si addition on the wear rate of the automotive alloys under dry, 3.5% NaCl solution and seawater environment are shown in Fig. 3. The wear rates were calculated from the weight loss and other parameters using Eqns. (i) and (ii) after sliding the samples 923.2 m against the stainless-steel disc at a constant velocity of 0.51 m/s and pressure of 2.55 MPa. It is conspicuous from Fig. 3 that for all environments, as the Si content increases in the alloys, the wear rate decreases accordingly at a level up to the eutectic composition of 12.7% Si. Beyond this composition, the wear rate increases to some extent for every sliding condition. When the aluminium alloy has a lower or trace amount of Si, intermetallics consisting of other constituent elements are formed, among them β-Al_3Mg_2 and MgAlCu are relevant to the discussion. The β-Al_3Mg_2 is gathered along the grain boundaries, which induces stress corrosion cracking [15]. Besides, a trace amount of Zn, which enters the alloy matrix as an impurity, often forms $Mg(ZnCuAl)_2$, which engenders preferential dissolution or dissolution of the precipitate [26]. Generally, in aluminium alloys, Al_2Cu formation provides a strengthening effect, consequently improving the wear properties of each tested alloy. However, increasing amounts of Si present in the alloy form the hard Mg_2Si intermetallic in the matrix that refine the α-Al grains and have excellent bonding capacity. As a result, additional Si in the alloy takes the Mg to form Mg_2Si intermetallic, and thus fewer amounts of β-Al_3Mg_2 and MgAlCu are formed in higher Si-added alloys. Previous investigations confirm the formation of these types of various intermetallics for Al-Si-Cu-Mg alloy through DSC and XRD studies [27-29].

The wear rate is lower in higher Si-doped alloy as Si addition refines the α-Al grains through the eutectic Si and forms the hard Mg_2Si intermetallic in the matrix with excellent interfacial bonding capacity. An increase in Si content brings about the further formation of Mg_2Si precipitates leading to improved strength and hardness of the alloy, which contributes to a lower wear rate. Additionally, Mg_2Si particles act as a load-bearing phase which reducing direct contact and protecting the matrix from the counter face during the sliding process. Beyond 12.7% Si content, the hypereutectic alloy does not follow the traditional positive correlation between hardness and wear resistance. At greater Si content, there might be a pull-out of primary silicon particles, leading to a three-body abrasive wear mechanism and a higher wear rate through the damage of the worn surface [30,31].

In the case of corrosive environments like 3.5% NaCl solution and seawater, the wear rate shows a similar trend, but

the intensity is different. For NaCl and seawater environments, higher wear rates are found for lower Si percentages. As previously discussed, Si provides a strengthening mechanism protecting the surface from damage, which does not function well when the silicon content is less. The β-Al_3Mg_2 phase present in the alloys with lower Si is preferentially attacked by corrosive environments [32]. Again, the presence of the MgAlCu phase in the alloy accelerates the corrosion as it acts as a galvanic cathode [33]. Besides, there are strong corrosive agents like chlorides present in both sodium chloride and seawater which are involved in further loss of material through corrosion reaction, which explains the higher rate of corrosion in these environments when the Si content is lower [34-37]. On top of that, seawater contains additional corrosive agents like HCO_3^-, which induces pitting corrosion removing material on the surface at heterogeneous spots [38]. There are phases of aluminium-iron in the alloys, such as Al_6Fe, and Al_3Fe, which are cathodic to the aluminium matrix [35,39,40]. These intermetallics induce a different chemical composition of the oxide layer. When this layer is exposed to seawater, these impurities create galvanic cells, which tend to promote pitting corrosion initiation, and progress rapidly [34]. These reasons explain the maximum corrosion rate under a seawater environment in hypo-eutectic alloys. On the other hand, the wear rate for every condition drastically abates by adding Si content into the alloys. In the region of 6.1 wt.% of Si, the corrosive media rate goes below that dry condition because the added Si forms Mg_2Si precipitates, which reacts with oxygen to produce layers of MgO and SiO_2, protecting the alloys from further corrosion [41,42]. This resistive effect of Mg_2Si increases with Si addition. Again, the seawater environment provides more protection than NaCl beyond 12.7 wt.% Si which can also be observed in Fig. 3. Generally, seawater has 3.5% salinity, and there are Na^+, K^+, Mg^{2+}, Ca^{2+}, Cl^-, SO_4^{2-}, HCO_3^-, NO_3^- *etc.* ions as components of seawater [38,43]. SO_4^{2-} hinders the inclusion of chloride ions into the oxide film, saving it from damage [44]. Besides, SO_4^{2-} tends to form aluminium and copper sulfate complexes on the surface of the alloy, which serve as a protective layer [45]. NO_3^- inhibits the corrosion process by lowering critical current passivation [46]. Furthermore, an additional layer of MgO is formed on the surface by the extra Mg^{2+} present in the seawater. Consequently, protection from corrosion is better established in a seawater environment than in a sodium chloride environment.

The friction coefficients of Al-based alloys of varying concentrations of Si under the wear tests in different sliding environments are presented in Fig. 4. It may be noted that the coefficient of friction decreases when the percentage of silicon increases into the alloys and this phenomenon alters beyond the eutectic composition of 12.7 wt.% Si. In alloy with low wt.% of Si, the coefficient of friction is high as phases like β-Al_3Mg_2, MgAlCu, and $Mg(ZnCuAl)_2$ promotes corrosion [26,32,33]. The decrease in coefficient of friction with the addition of Si may be attributed to the fact that more Mg_2Si is formed with the addition of silicon which enhances the mechanical strength of the alloys, and also reduces the amount of the β-Al_3Mg_2, MgAlCu, and $Mg(ZnCuAl)_2$ phases. As the mechanical property increases, the surface roughness should decrease improving the surface quality, which explains the lower coefficient of friction in higher Si-added alloys up to eutectic composition [9]. This decreasing trend is more prominent for the NaCl and seawater sliding environments as Mg_2Si formed in these alloys are converted into MgO and SiO_2 layers providing a lubrication effect. As previously discussed, additional layers composed of different ions are present in seawater conditions. Furthermore, as a moving fluid restricts solid-solid contact in the case of NaCl and seawater environments, the friction coefficient is less in these environments. Beyond eutectic composition, the friction coefficient rises suddenly because of the increased size of primary silicon particles as needle-like intermetallics [47]. The friction coefficient is also high for hypereutectic alloys in the corrosive environment due to increased pits and surface pinholes [48]. The friction coefficients for three different environments are close

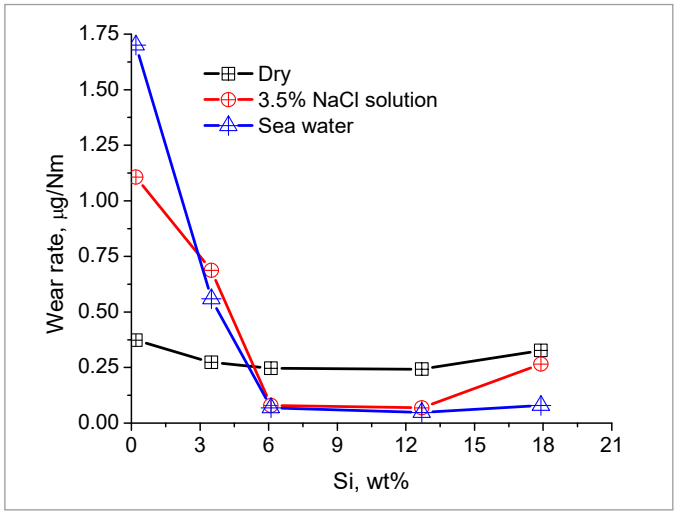

Fig. 3. Variation of wear rate with Si content into Al-based automotive alloys at applied pressure 2.55 MPa and sliding distance of 923.2 m at a velocity of 0.51 m/s under different environments

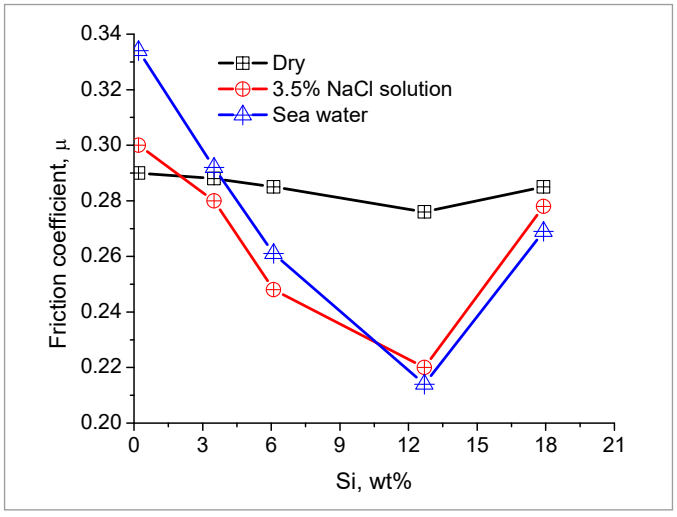

Fig. 4. Variation of coefficient of friction as a function of Si content into Al-based automotive alloys at applied pressure 2.55 MPa and sliding distance of 923.2 m at a velocity of 0.51 m/s under different environments

to each other. The oxide layer is thinned by more aggressive corrosion action in the hyper-eutectic alloy, making the surface condition almost the same under all environments [12].

3.3. Optical micrographic observation

The optical microscopic images of the surfaces of the experimental Al-based automotive alloys before and after wear in dry, 3.5% NaCl and seawater are shown in Fig. 5. Adequate information cannot be acquired from this type of unetched microscopic images. With the addition of Si, the α-Al phase with intermetallic particles scattered in intergranular and grain boundaries appear, and the eutectic phases increase. The amount of Si present can be identified by the lighter and darker spots on the surfaces prior to wear or corrosion. The darker spots represent the intermetallics containing Si and primary Si particles [49]. Furthermore, some blowholes and pinholes can be observed too, which might be the result of primary silicons. The interface temperature is increased at applied loads, which softens the material. As a result, thin metal layers are removed from the surfaces, causing the propagation of microcracks. This

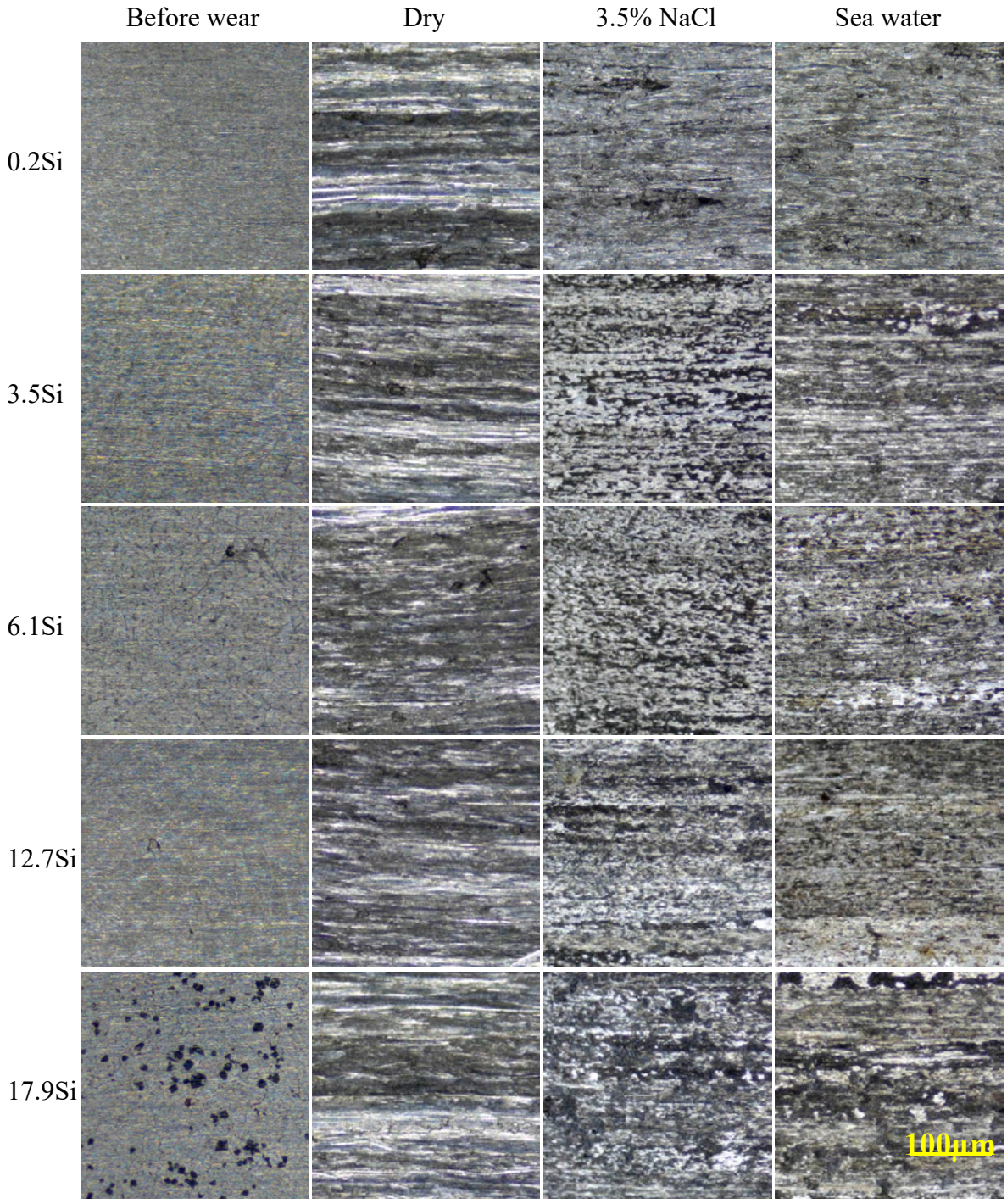

Fig. 5. Optical micrograph of worn surfaces of experimental alloys before and after wear for 923.2 m at an applied pressure of 2.55 MPa and sliding velocity of 0.51 m/s under different sliding environments

phenomenon is evident from the crater and tiny grooves visible in the figures of worn-out surfaces in the dry sliding condition. It is visible from Fig. 5 that in the dry condition, the wear marks on the worn surfaces are less in the alloys with higher Si content, as a higher amount of Si-rich Mg_2Si precipitates increase the strength of the alloys. Wear marks are relatively reduced because of the Si-rich phase, especially Mg_2Si reinforced particles, into the grain. Small, deep plowing and grooves with high delamination are observed in 17.9 wt.% Si added alloy.

In the case of NaCl and seawater corrosive environments, the surfaces of 0.2Si appear substantially demolished. The absence of Si lets the phases β-Al_3Mg_2, MgAlCu, $Mg(ZnCuAl)_2$, *etc.*, develop, which are often attacked by corrosion agents. Between the surfaces of 0.2Si doped alloys in these two environments, the one under seawater condition exhibits worse surface condition than the one under NaCl condition. The less damaged surface and more compact protective layers are observable for higher Si-added alloys. Nevertheless, 17.9 wt.% Si added alloy is an exception, as usual, depicting a more ruined surface state than those with lower silicon. The brittleness of phases of primary Si might be the reason [50].

Fig. 6 shows the optical micrographs of the abrasive dust particles generated from the wear test of the automotive alloys under the dry sliding condition. The granular shaped dust particles of the alloys are mixed with some chips created from the stainless-steel disc. Again, varying sizes and shapes of both the dust particles and stainless-steel chips in different experimental alloys are observed in the figure. A finer size of stainless-steel chips is found in alloys with more Si. As Si is added to the alloys, the intermetallics become finer, along with the refinement of grain structures, which increases hardness of the alloys. The increased the hardness and refined grains of the alloys are the reason for producing finer abrasive particles from the stainless-steel counter body. It is similar to that a grinding wheel produces fine particles with fine grit of the grinding wheel [51,52]. It can also be observed from Fig. 6 that the relative quantity of stainless-steel chips to the chips from the sample gets higher in alloys with higher Si percentages.

3.4. Scanning Electron Microscopy Observation

SEM microphotographs of base Alloy 1 and 12.7Si added Alloy 4 after wear for the above identical conditions are shown in Fig. 7. As 12.7Si added Alloy 4 shows the best wear performance in each environment, SEM and EDX observations are made between this alloy and the base Alloy 1, with a trace amount of Si. The figure depicts that the surfaces under the dry condition are mostly damaged from abrasive wear with oxides, which is dictated by scratches with random crevices and deep marks spread throughout. On the other hand, small, grooved cracks, and dislodged material, demonstrating a combination of mild and smooth abrasive grooves filled with oxides, are visible on the surface of 12.7Si added alloy, which proves that it has better wear resistance. The reason is that a higher level of Mg_2Si and β-Al_5FeSi is formed as intermetallics, strengthening and hardening the alloys as Si is increased [24,25]. Deep wear marks are also identifiable in the SEM images of Alloy 1 in corrosive environments. However, oxide layers are developed on the surface as corrosive products when exposed to corrosive environments, NaCl, and seawater. Besides aluminum, silicon, and magnesium oxides, an additional compact layer with Na^+ is formed on the surface in NaCl and seawater environments. These layers provide an intermediate film between the surfaces

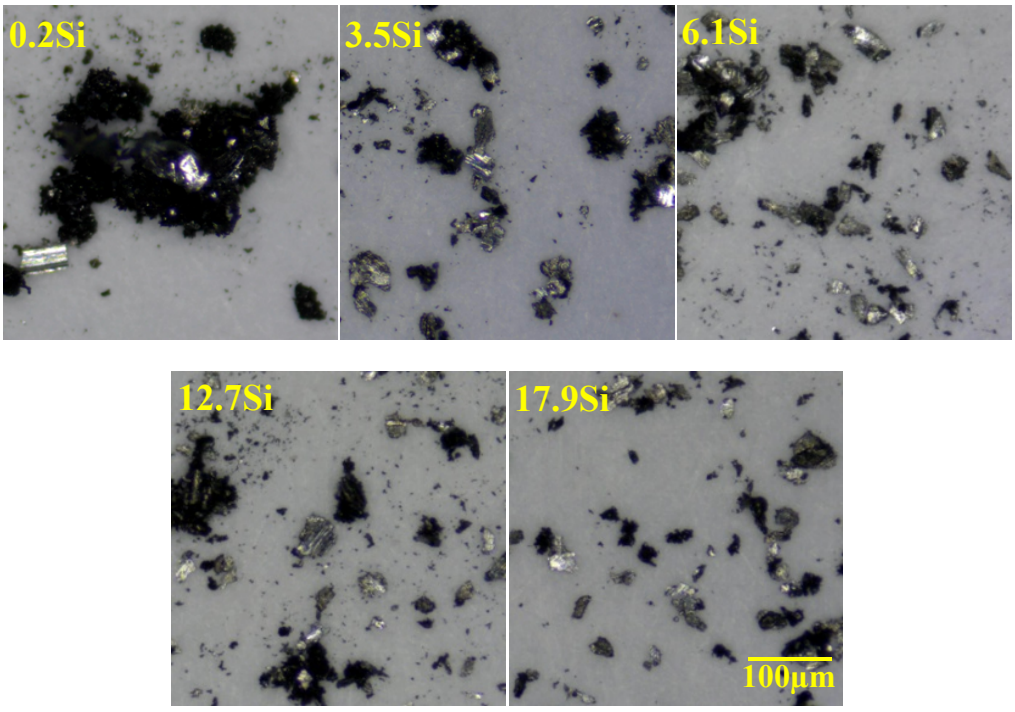

Fig. 6. Optical micrographs of the wear dust under the dry sliding condition

of the sample and the disc and minimize wear. Again, the smooth layers also reduce the friction between the surfaces. As a result, the surfaces of the alloys in corrosive environments have comparatively lower wear marks, which is evident from Figs. 7(c) to 7(f). Nevertheless, seawater has several additional elements absent in NaCl, which are involved in forming a thicker layer on the surface. Thus, comparing the three environments, the alloy under seawater has the fewest wear marks, identified in Figs. 7(e) and 7(f).

The wt.% of the components on the surface of Alloy 1 and 4 after corrosion under dry, 3.5% NaCl and seawater environments obtained from the EDX analysis is presented in TABLE 1. Observing the comparative percentages of Si and Al for among the three environments, it can be noted in both alloys that the wt.% of Si and Al is higher for the NaCl environment than for seawater and is highest for the dry condition. It indicates that additional Si particles remain on Alloy 1 and 4 under NaCl. The dry condition protects the surface and keeps more Al from erosion, because the

TABLE 1

The surface composition of the alloys after wear under dry, 3.5% NaCl, and the seawater environment, respectively, according to the EDX analysis

Environment	Alloy	Content, wt.%											
		Al	Si	O	Mg	Fe	Cu	Na	Cl	S	K	Ca	Br
Dry	Alloy 1	58.89	0.85	35.90	0.39	3.11	0.86	0	0	0	0	0	0
	Alloy 4	55.34	9.20	28.47	0.52	6.28	0.20	0	0	0	0	0	0
3.5% NaCl	Alloy 1	71.81	0.08	21.99	0.32	1.60	1.03	0.96	2.21	0	0	0	0
	Alloy 4	54.25	8.10	30.41	0.53	2.94	0.87	1.35	1.55	0	0	0	0
Seawater	Alloy 1	46.66	0	19.57	0.65	1.26	0.74	1.05	1.99	0.28	0.13	0.35	27.33
	Alloy 4	31.95	6.61	34.61	0.84	2.71	0.52	2.11	2.92	0.87	0.15	0.51	16.19

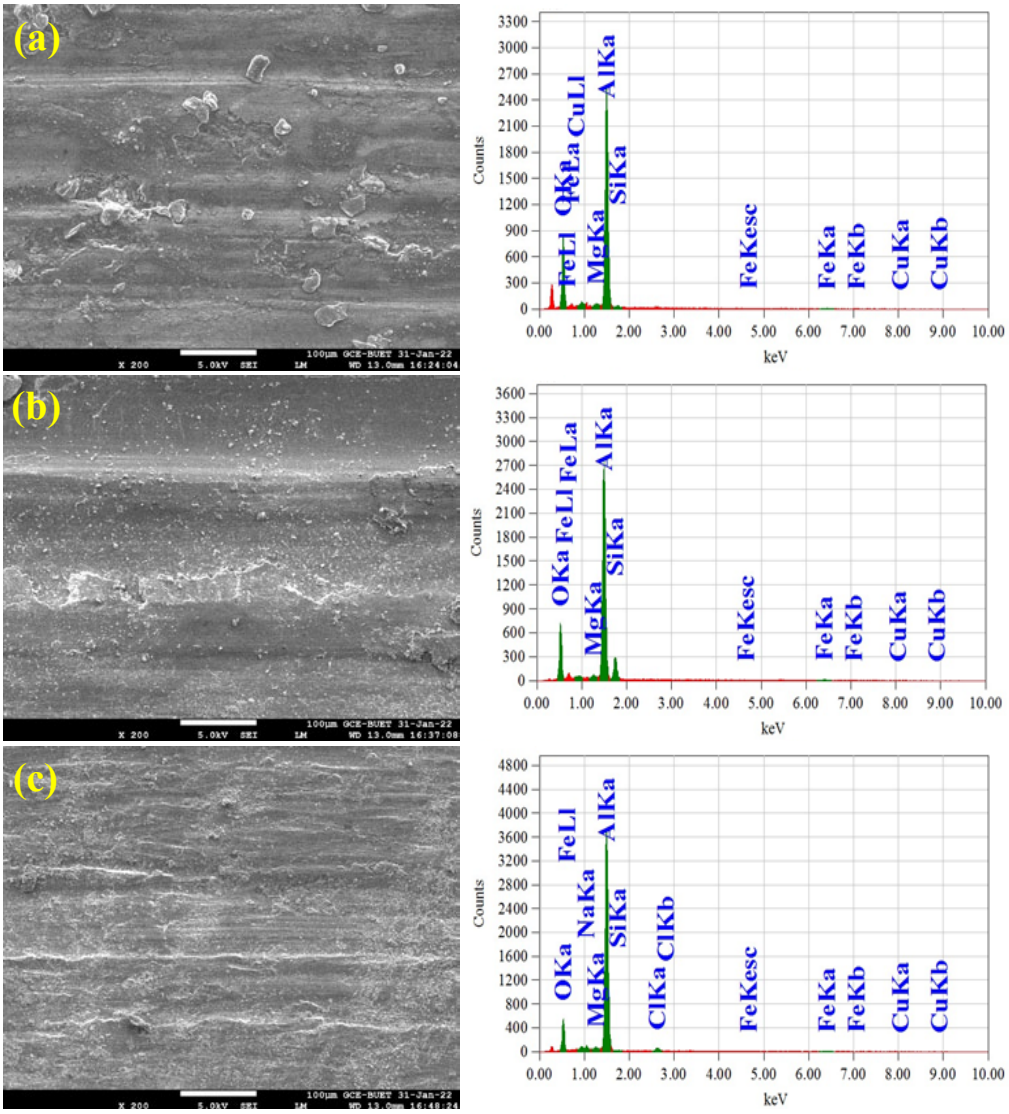

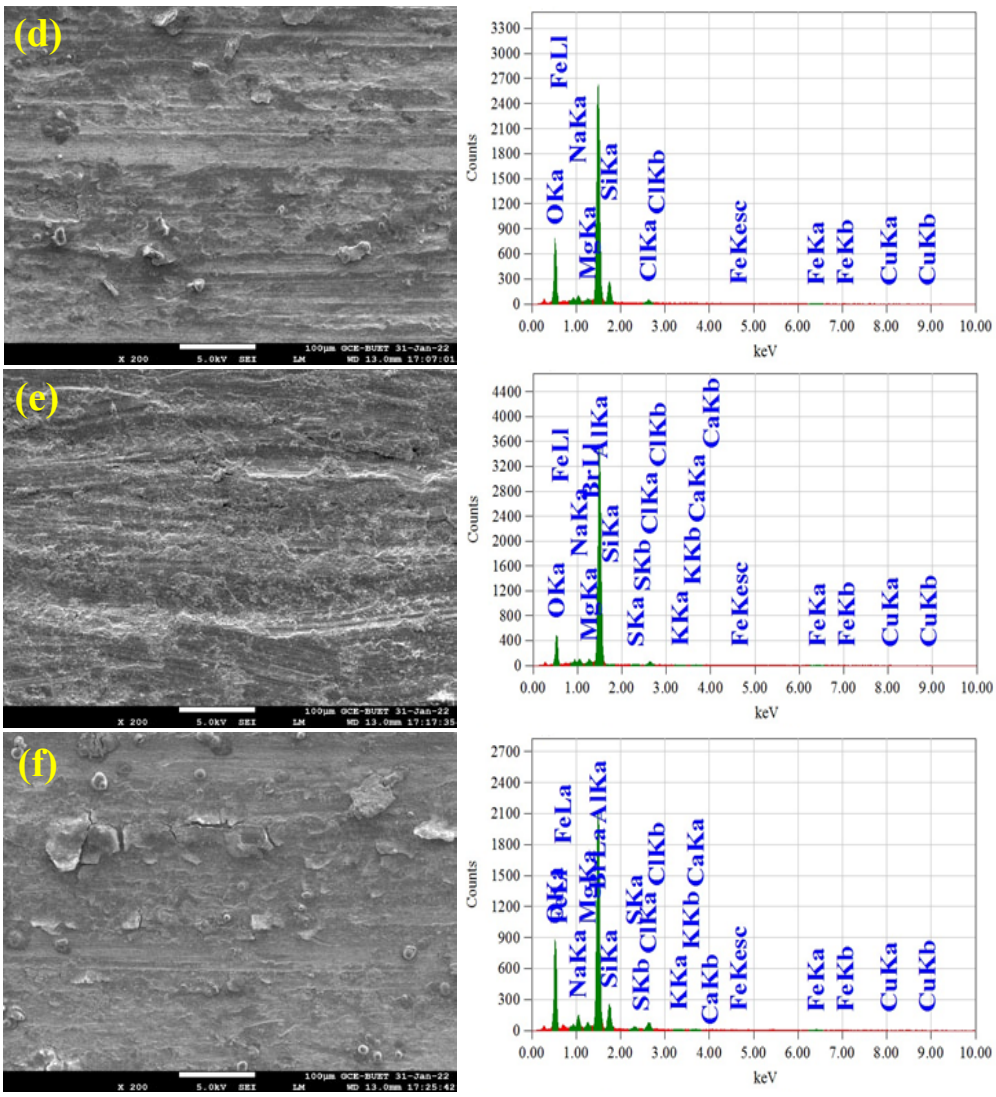

Fig. 7. SEM images and EDX spectra of the worn surfaces of (a) Alloy 1, (b) Alloy 4 under dry condition, (c) Alloy 1, (d) Alloy 4 under 3.5% NaCl solution environment, and (e) Alloy 1, (f) Alloy 4 under seawater environment for 923 m at an applied pressure of 2.55 MPa and 0.51 m/s sliding velocity

wear is less devastating in these two conditions. The Mg content is higher in Alloy 4 for every environment depicting an increased amount of MgO on the surface. Na, in the case of NaCl and seawater environment, and K, S, and Ca, for only the seawater environment, seem to exist in higher amounts in Alloy 4 than Alloy 1 as they are involved in forming protective layers. Again, the decreasing trend of Cu is observed in Alloy 4 for each environment as Cu atom increases the susceptibility to corrosion [53].

4. Conclusions

From the conducted investigations above, the following conclusions may be drawn.

1. Increasing silicon has led to more refined eutectic silicon and more Si-rich intermetallics in the Al-based automotive alloy matrix resulting in higher hardness. Consequently a higher level of Si in the alloy decreases the wear rate and friction coefficient under all three environments. Beyond the eutectic composition, the amount of primary silicon is increased, which weakens the matrix, so a higher wear rate and friction coefficient.
2. Trace or lower Si-containing alloys show a higher wear rate in corrosive environments. At higher wt.% of Si, the material loss reduces in the corrosive environments as several protective layers associated with Si are created. Seawater forms more layers with the additional elements present in it. The additional Si present forms oxides, which provide lubrication between the surfaces; hence, there is lower coefficient of friction. Beyond 12.7 wt%, the excess amount of primary Si results in a higher wear rate and coefficient of friction.
3. The optical micrography and SEM images indicate more deep grooves in the base alloy compared to 12.7 wt% alloys in all conditions. Again, oxide layers are visible in the SEM photographs for NaCl and seawater environments, which are thicker in seawater. The EDX spectra are congruent with these phenomena.

4. The optical micrography of the abrasive dust particles under the dry condition depicts that there are finer abrasive particles from the counter body for a higher percentage of Si, as the alloys with higher Si content are harder and finer grains.

REFERENCES

[1] F. Alshmri, Lightweight Material: Aluminium High Silicon Alloys in the Automotive Industry. Adv. Mater. Res. **774-776**, 1271-1276 (2013). DOI: https://doi.org/10.4028/www.scientific.net/AMR.774-776.1271

[2] M. Haghshenas, J. Jamali, Assessment of circumferential cracks in hypereutectic Al-Si clutch housings. Case Stud. Eng. Fail. Anal. **8**, 11-20 (2017). DOI: https://doi.org/10.1016/j.csefa.2016.11.003

[3] M. Javidani, D. Larouche, Application of cast Al–Si alloys in internal combustion engine components. Int. Mater. Rev. **59** (3), 132-158 (2014).
DOI: https://doi.org/10.1179/1743280413Y.0000000027

[4] M. GmbH, Piston materials, in: Pist. Engine Test., Vieweg+Teubner Verlag, Wiesbaden, 59-82, (2012).
DOI: https://doi.org/10.1007/978-3-8348-8662-0_4

[5] N. Kang, P. Coddet, C. Chen, Y. Wang, H. Liao, C. Coddet, Microstructure and wear behavior of in-situ hypereutectic Al–high Si alloys produced by selective laser melting. Mater. Des. **99**, 120-126 (2016). DOI: https://doi.org/10.1016/j.matdes.2016.03.053

[6] Z. Yang, X. He, B. Li, A. Atrens, X. Yang, H. Cheng, Influence of Si, Cu, B, and trace alloying elements on the conductivity of the Al-Si-Cu alloy. Materials (Basel). **15** (2), 426 (2022).
DOI: https://doi.org/10.3390/ma15020426

[7] L.F. Gomes, C.L. Kugelmeier, A. Garcia, C.A. Della Rovere, J.E. Spinelli, Influences of alloying elements and dendritic spacing on the corrosion behavior of Al–Si–Ag alloys. J. Mater. Res. Technol. **15**, 5880-5893 (2021).
DOI: https://doi.org/10.1016/j.jmrt.2021.11.043

[8] M.N. Ervina Efzan, H.J. Kong, C.K. Kok, Review: Effect of Alloying Element on Al-Si Alloys. Adv. Mater. Res. **845**, 355-359 (2013).
DOI: https://doi.org/10.4028/www.scientific.net/AMR.845.355

[9] A.A. Khan, M.R. Shoummo, M.S. Kaiser, Surface Quality of Fe, Ni, and Cr added Hyper-eutectic Al-Si Automotive Alloys under Up-milling and Down-milling Operation **6** (1), 9-22 (2022).
DOI: https://doi.org/10.17977/um016v6i12022p009

[10] W.S. Ebhota, T.-C. Jen, Intermetallics Formation and Their Effect on Mechanical Properties of Al-Si-X Alloys, in: Intermet. Compd. - Form. Appl., InTech. (2018).
DOI: https://doi.org/10.5772/intechopen.73188

[11] E. Tillová, D. Závodská, L. Kuchariková, M. Chalupová, J. Belan, Study of Bending Fatigue Properties of Al-Si Cast Alloy. Arch. Metall. Mater. **62** (3), 1591-1596 (2017).
DOI: https://doi.org/10.1515/amm-2017-0243

[12] M. Al Nur, A.A. Khan, S. Dev Sharma, M.S. Kaiser, Electrochemical corrosion performance of Si-doped Al-based automotive alloy in 0.1 M NaCl solution. J. Electrochem. Sci. Eng. **12** (3), 565-576 (2022). DOI: https://doi.org/10.5599/jese.1373

[13] M.G. Minciuna, P. Vizureanu, B. Jeż, A.V. Sandu, M. Nabialek, D.C. Achitei, Correlation between Microstructural and Electrochemical Properties of Al-Si Alloys. Arch. Metall. Mater. **67** (3), 1067-1070 (2022).
DOI: https://doi.org/10.24425/amm.2022.139704

[14] N.E. Udoye, O.S.I. Fayomi, A.O. Inegbenebor, Assessment of Wear Resistance of Aluminium Alloy in Manufacturing Industry – A Review. Procedia Manuf. **35**, 1383-1386 (2019).
DOI: https://doi.org/10.1016/j.promfg.2019.09.007

[15] M.S. Kaiser, M.A. Matin, K.M. Shorowordi, Role of magnesium and minor zirconium on the wear behavior of 5xxx series aluminum alloys under different environments. J. Mech. Energy Eng. **4** (3), 209-220 (2020).
DOI: https://doi.org/10.30464/jmee.2020.4.3.209

[16] D. Saber, R. Abdel-Karim, A.A. Kandel, K.A. El-Aziz, Corrosive Wear of Alumina Particles Reinforced Al–Si Alloy Composites. Phys. Met. Metallogr. **121** (2), 188-194 (2020).
DOI: https://doi.org/10.1134/S0031918X19120147

[17] S.M. Hsu, R. Munro, M.C. Shen, Wear in boundary lubrication. Proc. Inst. Mech. Eng. Part J, J. Eng. Tribol. **216** (6), 427-441 (2002). DOI: https://doi.org/10.1243/135065002762355343

[18] H. Ye, An Overview of the Development of Al-Si-Alloy Based Material for Engine Applications. J. Mater. Eng. Perform. **12** (3), 288-297 (2003).
DOI: https://doi.org/10.1361/105994903770343132

[19] M.S. Kaiser, M.R. Basher, A.S.W. Kurny, Effect of scandium on microstructure and mechanical properties of cast Al-Si-Mg alloy. J. Mater. Eng. Perform. **21** (7), 1504-1508 (2012).
DOI: https://doi.org/10.1007/s11665-011-0057-3

[20] S. Toschi, Optimization of A354 Al-Si-Cu-Mg Alloy Heat Treatment: Effect on Microstructure, Hardness, and Tensile Properties of Peak Aged and Overaged Alloy. Metals (Basel). **8** (11), 961 (2018).
DOI: https://doi.org/10.3390/met8110961

[21] A.A. Razin, D.S. Ahammed, M. Al Nur, M.S. Kaiser, Role of Si on machined surfaces of Al- based automotive alloys under varying machining parameters. J. Mech. Energy Eng. **6** (1), 43-52 (2022).
DOI: https://doi.org/10.30464/jmee.2022.6.1.43

[22] M.S. Kaiser, S.H. Sabbir, M.S. Kabir, M.R. Soummo, M. Al Nur, Study of mechanical and wear behaviour of hyper-eutectic Al-Si automotive alloy through Fe, Ni and Cr addition. Mater. Res. **21** (4), (2018).
DOI: https://doi.org/10.1590/1980-5373-mr-2017-1096

[23] P.-F. Liu, L. Miao, Z. Deng, J. Zhou, Y. Gu, S. Chen, H. Cai, L. Sun, S. Tanemura, Flame-treated and fast-assembled foam system for direct solar steam generation and non-plugging high salinity desalination with self-cleaning effect. Appl. Energy. **241**, 652-659 (2019).
DOI: https://doi.org/10.1016/j.apenergy.2019.02.030

[24] I.J. Polmear, Light Alloys-Metallurgy of the Light Metals, 3rd ed., Arnold, London, (1995).

[25] M.S. Kaiser, A. Towsif, S. Reaz Ahmed, Effect of Post-weld Thermal Treatment on Mechanical Properties of Welded Aluminum-Alloy Engine Head. J. Mater. Eng. Perform. **26** (8), 4148-4154 (2017). DOI: https://doi.org/10.1007/s11665-017-2846-9

[26] Q. Meng, G.S. Frankel, Effect of Cu Content on Corrosion Behavior of 7xxx Series Aluminum Alloys. J. Electrochem. Soc. **151** (5), B271 (2004). DOI: https://doi.org/10.1149/1.1695385

[27] Y.J. Kang, J.H. Kim, J. Il Hwang, K.A. Lee, Effect of T6 heat treatment on the scratch wear behavior of extruded Al-12WT.%Si alloy. Arch. Metall. Mater. **64** (2), 617-622 (2019). DOI: https://doi.org/10.24425/amm.2019.127588

[28] B. Zhang, L. Zhang, Z. Wang, A. Gao, Achievement of High Strength and Ductility in Al–Si–Cu–Mg Alloys by Intermediate Phase Optimization in As-Cast and Heat Treatment Conditions. Materials (Basel). **13** (3), 647 (2020). DOI: https://doi.org/10.3390/ma13030647

[29] V. Raghavan, Al-Cu-Mg-Si (Aluminum-Copper-Magnesium-Silicon). J. Phase Equilibria Diffus. **28** (2), 198-200 (2007). DOI: https://doi.org/10.1007/s11669-007-9046-5

[30] A.K. Prasada Rao, K. Das, B.S. Murty, M. Chakraborty, Effect of grain refinement on wear properties of Al and Al–7Si alloy. Wear. **257** (1-2), 148-153 (2004). DOI: https://doi.org/10.1016/j.wear.2003.10.017

[31] G.E. Toten, Lubrication and Wear Technology, 18th ed., ASM Handbook, Materials Park, Ohio, USA, 1992

[32] Y. Zhu, D.A. Cullen, S. Kar, M.L. Free, L.F. Allard, Evaluation of Al3Mg2 Precipitates and Mn-Rich Phase in Aluminum-Magnesium Alloy Based on Scanning Transmission Electron Microscopy Imaging. Metall. Mater. Trans. A. **43** (13), 4933-4939 (2012). DOI: https://doi.org/10.1007/s11661-012-1354-7

[33] X.W. Wang, W. Wang, W. Chen, D.M. Chen, Effect of Al addition and heat treatment on the microstructures and corrosion resistance of Mg-Cu alloys. J. Mater. Sci. Technol. **98**, 219-232 (2022). DOI: https://doi.org/10.1016/j.jmst.2021.05.010

[34] H. Ezuber, A. El-Houd, F. El-Shawesh, A study on the corrosion behavior of aluminum alloys in seawater. Mater. Des. **29** (4), 801-805 (2008). DOI: https://doi.org/10.1016/j.matdes.2007.01.021

[35] Z. Szklarska-Smialowska, Pitting corrosion of aluminum. Corros. Sci. **41** (9), 1743-1767 (1999). DOI: https://doi.org/10.1016/S0010-938X(99)00012-8

[36] W.M. Carroll, C.B. Breslin, Stability of passive films formed on aluminium in aqueous halide solutions. Br. Corros. J. **26** (4), 255-259 (1991). DOI: https://doi.org/10.1179/000705991798269035

[37] B.A. Shaw, G.D. Davis, T.L. Fritz, B.J. Rees, W.C. Moshier, The Influence of Tungsten Alloying Additions on the Passivity of Aluminum. J. Electrochem. Soc. **138** (11), 3288-3295 (1991). DOI: https://doi.org/10.1149/1.2085404

[38] A.K. Behera, G.J. Chakrapani, S. Kumar, N. Rai, Identification of seawater intrusion signatures through geochemical evolution of groundwater: a case study based on coastal region of the Mahanadi delta, Bay of Bengal, India. Nat. Hazards. **97** (3), 1209-1230 (2019). DOI: https://doi.org/10.1007/s11069-019-03700-6

[39] A.S. Fouda, F.S. Mohamed, M.W. El-Sherbeni, Corrosion Inhibition of Aluminum–Silicon Alloy in Hydrochloric Acid Solutions Using Carbamidic Thioanhydride Derivatives. J. Bio- Tribo-Corrosion. **2** (2), 11 (2016). DOI: https://doi.org/10.1007/s40735-016-0039-y

[40] J.R. Davis, Corrosion of Aluminum and Aluminum Alloys, ASM International, 1999

[41] R. Escalera-Lozano, M.I. Pech-Canul, M.A. Pech-Canul, M. Montoya-Davila, A. Uribe-Salas, The role of Mg2Si in the corrosion behavior of Al-Si-Mg alloys for pressureless infiltration. Open Corros. J. **3** (1), 73-79 (2010). DOI: https://doi.org/10.2174/1876503301003010073

[42] A.A. Khan, M.S. Kaiser, Electrochemical corrosion performance of eutectic Al-Si automotive alloy in 0.1 M and 0.2 M NaCl solution. IOP Conf. Ser. Mater. Sci. Eng. **1248** (1), 012031 (2022). DOI: https://doi.org/10.1088/1757-899X/1248/1/012031

[43] A.G. Dickson, C. Goyet, Handbook of methods for the analysis of the various parameters of the carbon dioxide system in sea water. Version 2, Oak Ridge, TN, (1994). DOI: https://doi.org/10.2172/10107773

[44] W.-J. Lee, S.-I. Pyun, Effects of sulphate ion additives on the pitting corrosion of pure aluminium in 0.01 M NaCl solution. Electrochim. Acta. **45** (12), 1901-1910 (2000). DOI: https://doi.org/10.1016/S0013-4686(99)00418-1

[45] B.W. Samuels, K. Sotoudeh, R.T. Foley, Inhibition and Acceleration of Aluminum Corrosion. Corrosion **37** (2), 92-97 (1981). DOI: https://doi.org/10.5006/1.3593852

[46] P. Sureshkumar, T. Jagadeesha, L. Natrayan, M. Ravichandran, D. Veeman, S.M. Muthu, Electrochemical corrosion and tribological behaviour of AA6063/Si3N4/Cu(NO3)2 composite processed using single-pass ECAPA route with 120° die angle. J. Mater. Res. Technol. **16**, 715-733 (2022). DOI: https://doi.org/10.1016/j.jmrt.2021.12.020

[47] N. Kang, M. EL Mansori, A new insight on induced-tribological behaviour of hypereutectic Al-Si alloys manufactured by selective laser melting. Tribol. Int. **149**, 105751 (2020). DOI: https://doi.org/10.1016/j.triboint.2019.04.035

[48] M.G. Mueller, M. Fornabaio, A. Mortensen, Silicon particle pinhole defects in aluminium-silicon alloys. J. Mater. Sci. **52** (2), 858-868 (2017). DOI: https://doi.org/10.1007/s10853-016-0381-y

[49] M.S. Kaiser, M.R. Qadir, S. Dutta, Electrochemical Corrosion Performance Of Commercially Used Aluminium Engine Block And Piston In 0.1 M NaCl. J. Mech. Eng. **45** (1), 48-52 (2015). DOI: https://doi.org/10.3329/jme.v45i1.24384

[50] V.V.K. Narayan Prabhu, Review of Microstructure Evolution in Hypereutectic Al–Si Alloys and its Effect on Wear Properties. Trans. Indian Inst. Met. **67** (1), 1-18 (2014). DOI: https://doi.org/10.1007/s12666-013-0327-x

[51] Y. Zedan, A.M. Samuel, H.W. Doty, V. Songmene, F.H. Samuel, Effects of Trace Elements on the Microstructural and Machinability Characteristics of Al–Si–Cu–Mg Castings. Materials (Basel). **15** (1), 377 (2022). DOI: https://doi.org/10.3390/ma15010377

[52] X. Chen, T.T. Öpöz, Effect of different parameters on grinding efficiency and its monitoring by acoustic emission. Prod. Manuf. Res. **4** (1), 190-208 (2016). DOI: https://doi.org/10.1080/21693277.2016.1255159

[53] W.J. Liang, P.A. Rometsch, L.F. Cao, N. Birbilis, General aspects related to the corrosion of 6xxx series aluminium alloys: Exploring the influence of Mg/Si ratio and Cu. Corros. Sci. **76**, 119-128 (2013). DOI: https://doi.org/10.1016/j.corsci.2013.06.035